The Influence of the pH on the Reaction Mechanism of Water Oxidation by a Ru(bda) catalyst

Jesús A. Luque-Urrutia,[‡] Miquel Solà*[,‡] and Albert Poater*[,‡]

[‡]Institut de Química Computacional i Catàlisi and Departament de Química, Universitat de Girona, C/ Maria Aurèlia Capmany, 69, 17003 Girona, Catalonia, Spain

KEYWORDS: Water oxidation catalysis, ruthenium complex, DFT, redox potential, O_2 formation, reaction mechanism, di-carboxylate

ABSTRACT: Recent results of Concepcion's group (*Chem. Commun.* **2015**, *51*, 4105) on water oxidation catalysis (WOC) by a ruthenium complex suggest that, at pH = 8, O_2 release takes place after formation of a rhomboid bis(μ-oxo)-Ru^{V}_2 species and not after generation of the typical μ-η^1:η^1-peroxo-Ru^{IV}_2 intermediate, coming from the coupling of two Ru^{V}=O moieties (I2M mechanism), which is widely accepted to be formed at pH = 1. To analyze the differences between the reaction mechanisms of this WOC at different pHs, we performed DFT calculations of the full mechanism at pH = 1 and 8 of the WOC process catalyzed by the 2,2'-bipyridine-6,6'-dicarboxylate Ru complex. At pH = 8, we found that barriers leading to the hypothetic formation of rhombic $Ru^{V}_2O_2$ species are higher than those involved in the canonical I2M mechanism. The rate determining step at the latter pH is found to be the dimer formation while the bond cleavage for the O_2 liberation process is barrierless. The computational results confirm that the most common I2M mechanism is preferred at both pHs, as the new proposal comprising formation of bis(μ-oxo)-Ru^{V}_2 species involves higher energy barriers.

INTRODUCTION

The production of hydrogen has become one of the main modern research focus due to its potential as energy source. Since it is costly and dangerous to maintain tanks of pressurized hydrogen for our daily use, *in situ* production is currently under investigation [1,2,3]. Ideally, H_2 is obtained from water because of its abundance, low risk and cost for its storage and manipulation [4]. But more importantly, it represents a carbon-free production of energy, and does not make use of fossil fuel sources.

In 2012, Sun, Llobet, Privalov *et al.* designed the 2,2'-bipyridine-6,6'-dicarboxylate Ru catalyst, [Ru(bda)(pic)$_2$] (Figure 1) [5]. This, and other Ru catalysts[6,7,8], mimic the Photosystem II catalytic activity, showing a great efficiency in water oxidation catalysis (WOC). This catalyst is able to undertake proton coupled electron transfer (PCET) reactions like other ruthenium complexes [9,10]. In most cases, these Ru complexes initiate their catalytic activity rearranging from 6- to 7-coordination [11].

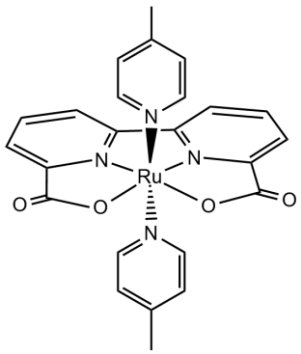

Figure 1. The [Ru^{II}(bda)(pic)$_2$] catalyst studied in this work.

Two possible mechanisms for O–O bond formation in WOC have been proposed, namely, water nucleophilic attack (WNA) [12,13,14] and coupling between 2 M-O centers (I2M) (Figure 2) [15,16,17,18,1 9]. Several studies have shown that the I2M pathway is the preferred mechanism for this catalyst [16,20,21].

Even though previous works suggested that there might be a sort of equilibrium between both mechanisms, as previously described for Ru(bda) complexes [22], the WNA was found energetically disfavored [16]. Despite the rather good efficiency of the [Ru(bda)(pic)$_2$] catalyst [23], further research is needed to fully understand the reaction mechanism of this seven coordinated molecular ruthenium water oxidation catalyst [24,25]. Usually, the reaction follows an I2M between two monomers, forming a Ru-O-O-Ru bond [26,27]. However, Concepcion *et al.* [28,29] suggested another route at pH = 8 involving the formation of a Ru-O-Ru central motif followed by a bis(μ-oxo)-Ru^{V}_2 species with a rhomboid metal core (see Scheme 1).

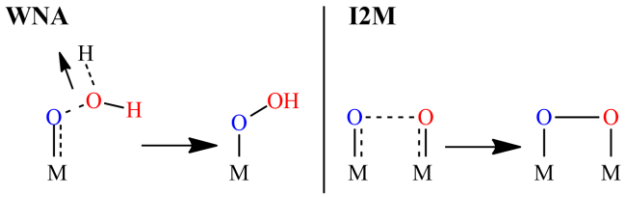

Figure 2. WNA and I2M mechanisms for the O-O bond formation.

Since two different mechanisms for the two pHs were proposed, in this work, we aim to unveil the reaction mechanism of the WOC catalyzed by [Ru(bda)(pic)$_2$] at pH 1 and 8 to confirm whether the Concepcion *et al.* proposal at pH = 8 is competitive with the widely accepted I2M mechanism. Additionally, comprehending the reaction mechanism on a molecular scale may help to diminish the byproducts of the reaction and to improve the current turnover number (TON) and turnover frequency (TOF) of this reaction [30,31].

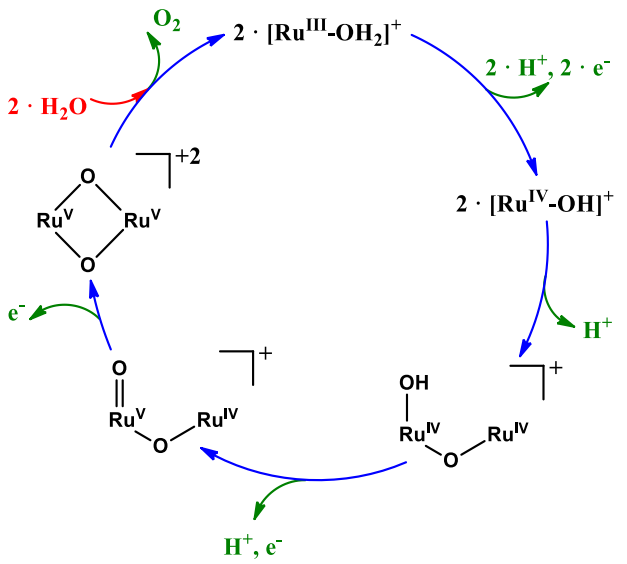

Scheme 1. Proposed water oxidation mechanism for [Ru(bda)(pic)$_2$] (abbreviated as Ru) at pH = 8. Adapted from Concepcion *et al.* [28].

COMPUTATIONAL DETAILS

All DFT calculations were performed with the Gaussian09 set of programs [32] using the M06-L functional [33,34]. The electronic configuration of the molecular systems was described with the standard split-valence basis set with a polarization function of Ahlrichs and co-workers for H, C, N, O, P (SVP keyword in Gaussian09) [35]. Ruthenium was described by the small-core quasi-relativistic Stuttgart/Dresden effective core potential, with an associated valence basis set (standard SDD keyword in Gaussian09) [36]. The geometry optimizations were performed without symmetry constraints, and the characterization of the local stationary points was carried out by analytical frequency calculations. These frequencies were used to calculate unscaled zero-point energies (ZPEs) as well as thermal corrections and entropy effects at 298.15 K and 1354 atm [37] by using the standard statistical mechanics relationships for an ideal gas. The pressure of 1354 atm was considered in our calculations based on the work of Martin *et al.* [37], who determined that this pressure simulates the experimental density of liquid water for the ideal water gas including the deformations performed by the surrounding water solvent in aqueous media [38]. We obtained the solvent energies by single-point calculations on the optimized geometries with the triple-ζ basis set of Weigend and Ahlrichs for main-group atoms (TZVP keyword in Gaussian09) [39], whereas for ruthenium the SDD basis set was employed. Solvent effects were included with the polarizable continuous solvation model PCM using H_2O as a solvent [40,41]. The reported Gibbs energies in this work are electronic energies obtained at the M06-L/TZVP~sdd//M06-L/SVP~sdd level of theory corrected with zero-point energies, thermal corrections, and entropy effects evaluated at 298.15 K and 1354 atm at the M06-L/SVP~sdd level and including solvation Gibbs energies calculated with the M06-L/TZVP~sdd//M06-L/SVP~sdd method.

To evaluate the pK_a values of our transition metal complexes, we used the scheme of Durrant and Gilson [42]. In particular, pK_a values in this work were obtained through their formula for hydroxy acids (eq. 1):

$$AOH \rightarrow AO^- + H^+$$

$$pK_a = 0.275 \cdot \Delta E - 4.20 \quad (1)$$

where ΔE refers to the reaction energy in kcal/mol obtained from the electronic energies in solution. Application of Eq. (1) to the related 2,2'-bipyridine-6,6'-diphosphonate Ru catalyst yields a pK_a of 4.13 and 4.30 (protons of different phosphonate groups) not far from the experimental value of ~4.1 for the double deprotonation of the phosphonate group [43]. For the energy of the solvated proton H_3O^+ we used -258.4 kcal/mol [42].

We represent redox reactions [44] using the following equation:

$$A^+ + e^- \rightarrow A$$

$$\varepsilon^0_{red} = \frac{\Delta G}{-nF} - \varepsilon^0_{SHE} \quad (2)$$

Where ΔG is the Gibbs energy of the reaction. The SHE refers to the absolute potential of the Standard Hydrogen Electrode (4.28 V) [45] in water, n refers to the number of electrons transferred and F is the Faraday constant. Energies are given in kcal/mol and the reduction potential ε^0_{red} in V.

Since PCET reactions include ΔG_{H^+}, we used the following formula to determine its reduction potential:

$$Ru^nOH + e^- + H^+ \rightarrow Ru^{n-1}OH_2$$

$$\varepsilon^0_{red} = \frac{\Delta G_{Ru^{n-1}OH_2} - \Delta G_{Ru^nOH} - 0.5 \cdot \Delta G_{H_2}}{-nF} \quad (3)$$

Where we used the Gibbs energy of the calculated solvated hydrogen molecule. Additionally, since the reduction potentials of PCET reactions are dependent on the pH, we included the -0.059 · pH correction obtained at 298.15 K [46]. For a more detailed description, see the SI.

Since the formal charges on ruthenium are in some cases arguable, we undertook an Effective Oxidation State (EOS) analysis to assign the oxidation state of the Ru atom in intermediates and transition states, via the in-house software APOST-3D [47]. Using the Topological Fuzzy Voronoi Cells (TFVC) 3D-space partitioning method and a 70 x 434 atomic grid for the numerical integration, we obtained the Reliability index ($R_\sigma(\%)$) calculated using the occupancies of the last occupied (λ^σ_{LO}) and first unoccupied (λ^σ_{FU}) effective atomic orbitals as shown in eq. 4:

$$R_\sigma(\%) = 100 \cdot \min(1, max(0, \lambda^\sigma_{LO} - \lambda^\sigma_{FU} + 1/2)) \quad (4)$$

This index reveals the reliability of the oxidation states assigned to the chosen atoms or molecular fragments. For R > 65-70%, the oxidation state can be assigned with confidence.

RESULTS AND DISCUSSION

In Scheme 2, we report all possible routes for the WOC mechanism catalyzed by the 2,2'-bipyridine-6,6'-dicarboxylate Ru catalyst. Further details are given in Scheme 3 (pH = 1) and Scheme 4 (pH = 8). Throughout this work, we named our complexes as $^{2S+1}\mathbf{X}^{+q}$, where S is the spin and q the charge of species **X**. It is worth noting that for all species with even number of electrons we have computed the closed-shell singlet, the open-shell singlet, the triplet, and the quintuplet electronic states. We found that in all cases the closed-shell singlet is favored, except for the TS of the I2M coupling between two Ru^VO units (^{2}**12**$^{+1}$+^{2}**12**$^{+1}$ in Scheme 3), for which the open-shell singlet state is lower in energy, and for the Ru^{IV}=O species, for which the triplet is the ground state in agreement with the calculations done by Concepcion and coworkers [12]. Further, for species with odd number of electrons, we tested both the doublet and quadruplet electronic states, the latter being higher in energy in all cases. In this work, we represent only the lowest energy electronic states for the sake of clarity.

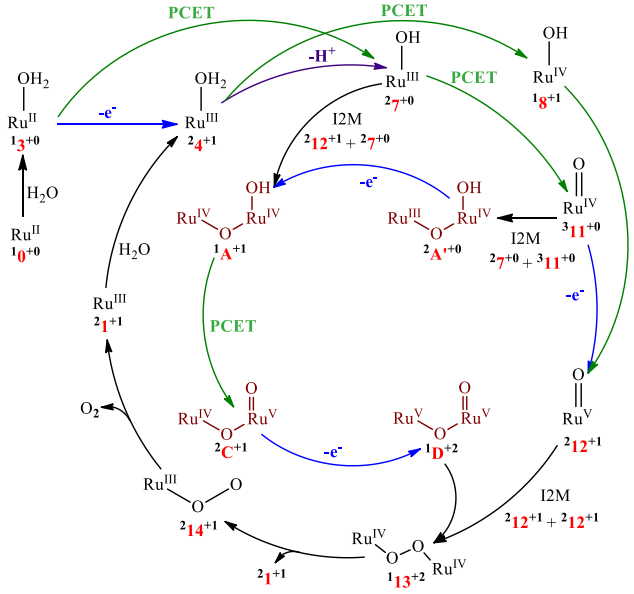

Scheme 2. General reaction mechanism for the water oxidation catalysis by 2,2'-bipyridine-6,6-dicarboxylate Ru catalyst. Arrows in blue denote

oxidation processes, in purple deprotonation, and in green proton-coupled electron transfers.

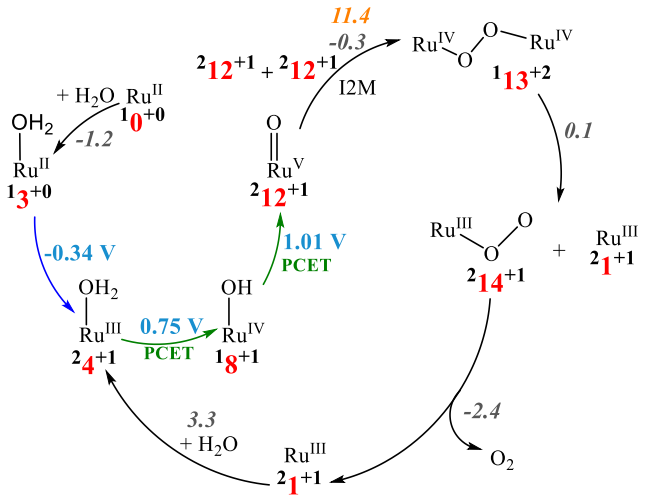

Scheme 3. Mechanism for the Ru-bda catalyst at pH = 1; PCETs in green; Gibbs energy barriers in orange; reduction potentials in light blue; Gibbs reaction energies in grey. Energies are given in kcal/mol and oxidation potentials in V. Arrows in blue denote oxidation processes and in green proton-coupled electron transfers.

We have chosen intermediate $^{2}\mathbf{4}^{+1}$ as the catalyst while $^{1}\mathbf{0}^{+0}$ and $^{1}\mathbf{3}^{+0}$ (represented in Figure 1) have been defined as precatalysts. Comparing our structural data with those given in the Supporting Information (SI) by Concepcion *et al.* [28] we determined that bond lengths of our structures are similar to theirs, the biggest absolute error being 0.066 Å. Two experiments were performed by Concepcion's group at pH = 1, one was the addition of excess CAN (Cerium Ammonium Nitrate), *i.e.* the oxidant in the media at pH = 1, we ensure a minimal reduction potential of 1.72 V [48,49]; and the other was the cyclic voltammetry. For the sake of clarity, we define the CAN potential as the maximum to perform the different oxidation reactions thus; we do not consider reactions with higher potentials. We have tried many different pathways and possibilities, and we represent in Scheme 3 the most likely reaction mechanism at pH = 1. A full account of all different reaction paths can be found in the SI.

The oxidation state on ruthenium atoms (for all studied complexes in this work) ranges from II to V as we show in Table 1 with their respective reliability indexes.

Table 1. Oxidation states (OS) and their corresponding Reliability indexes (R%) for some the molecules represented in this work.

Mol.	**0**	**1**	**4**	**7**	**8**	**11**	**12**	**A**
OS	II	III	III	III	IV	IV	V	IV&IV
R%	90.4	86.0	87.0	92.8	85.7	59.8	50.9	78.1
Mol.	**A'**	**C**	**D**	**13**	**14**	**7+12 TS**	**7+11 TS**	**12+12 TS**
OS	III&IV	IV&V	IV&IV	IV&IV	III	IV&IV	III&IV	IV&IV
R%	63.9	60.3	63.3	81.1	85.0	75.3	78.3	73.6

As we can see, $^{3}\mathbf{11}^{+0}$, $^{2}\mathbf{12}^{+1}$, $^{2}\mathbf{A'}^{+0}$, $^{2}\mathbf{C}^{+1}$ and $^{1}\mathbf{D}^{+2}$ are the most problematic since their R% are not high enough to determine with total confidence the OS of their Ru atoms. This is due to the close proximity in energy between the occupied and unoccupied orbitals, *i.e.* molecule $^{2}\mathbf{12}^{+1}$ λ_{LO}^{σ} has an assigned occupancy of 0.440 e$^-$ while the λ_{FU}^{σ} an occupancy of 0.448 e$^-$. This difference implies that it is not possible to determine with total certainty whether the oxo group fragment OS is considered -2 (thus Ru fragment +5) or -1 (thus Ru fragment +4). It is worth noting that out of these five complexes, only complexes $^{3}\mathbf{11}^{+0}$ and $^{2}\mathbf{12}^{+1}$ are relevant in the reaction mechanisms found to be operative (*vide infra*).

Moving to the mechanism discussion (Scheme 3), starting from $^{1}\mathbf{0}^{+0}$, we believe that, first, a water molecule interacts with $^{1}\mathbf{0}^{+0}$ in the second coordination sphere to form $^{1}\mathbf{3}^{+0}$ and releasing 1.2 kcal/mol. The same energy value was reported by Concepcion *et al.* [12] for the coordination of water to Ru^{II}. In the experiments by their group, they observed that at pH = 1 there were two oxidation steps at 0.85 V and 1.10 V [50]. Our calculations indicate that these two steps are two PCET processes at 0.75 V and 1.01 V. We also considered the oxidations and deprotonations separately, but due to the low pH, the intermediates found would re-protonate. Comparing the proposal by Concepcion *et al.* [12] and our work, we obtained similar results up to the formation of $^{2}\mathbf{12}^{+1}$. Furthermore, the calculations are in agreement with the detection of this type of intermediate by Copéret, Pushkar *et al.* [51].

Once we form $^{2}\mathbf{12}^{+1}$, a coupling between 2 M-O sites occurs. Formation of $^{1}\mathbf{13}^{+2}$, Ru^{IV}-O-O-Ru^{IV}, through an I2M mechanism is exergonic by 0.3 kcal/mol and has an estimated Gibbs energy barrier of 11.4 kcal/mol. The corresponding transition state displays an open-shell singlet character and indeed, it is a bimolecular oxyl radical coupling of two [Ru^{V}=O]$^{+}$ species as Concepcion *et al.* [28] and Sun *et al.* [5] groups reported. The highest in energy structure used to estimate the energy barrier for an O-O frozen bond distance of 1.90 Å was obtained with a linear transit procedure by changing the O-O distance with steps of 0.1 Å. We used this estimate, as we were unable to locate the exact transition state. It is worth noting that the same linear transit procedure leads to an error of less than 0.1 kcal/mol for similar transition states with a Ru-bda complex [52]. Moreover, the barrier fits into the expected energy range at our given conditions [53]. The interaction between two $^{2}\mathbf{12}^{+1}$ monomers giving the dimer $^{1}\mathbf{13}^{+2}$ turns out to be the rate determining step (rds) of the process at pH = 1 [54]. Following the mechanism, we studied the dimer cleavage. From the linear transit carried out following the same procedure as for the search of the I2M transition state, we concluded that the $^{1}\mathbf{13}^{+2}$ → $^{2}\mathbf{14}^{+1}$+$^{2}\mathbf{1}^{+1}$ transformation is a barrierless dissociative process. Once the Ru^{V}-η^{1}-O$_2$ compound $^{2}\mathbf{14}^{+1}$ is obtained, the release of molecular oxygen, again barrierless and exergonic by 2.4 kcal/mol, leads to compound $^{2}\mathbf{1}^{+1}$, which then hydrates to regenerate the active catalyst $^{2}\mathbf{4}^{+1}$.

At pH = 8 (Scheme 4), the mechanism shows some differences. The transformation from $^{1}\mathbf{0}^{+0}$ to $^{2}\mathbf{4}^{+1}$ does not occur. Instead, the water coordination leads to $^{1}\mathbf{3}^{+0}$, and then via a PCET directly to $^{2}\mathbf{7}^{+0}$. This compound $^{2}\mathbf{7}^{+0}$ was characterized using X-ray cristallography by Sun and coworkers,[55] who also stated that at pH 7 and above, two molecules of $^{2}\mathbf{7}^{+0}$ disproportionate into $^{3}\mathbf{11}^{+0}$ and $^{1}\mathbf{3}^{+0}$. Reported Pourbaix diagram by Concepcion's group [28] show that at pH > 6, the line of the pH dependent reaction of $^{1}\mathbf{3}^{+0}$ to $^{3}\mathbf{11}^{+0}$ crosses below the line of the pH independent reaction of $^{1}\mathbf{3}^{+0}$ to $^{2}\mathbf{4}^{+1}$. As a consequence, they observed a 2e$^-$/2H$^+$ step in their experiments. Actually, this step could be considered to gather the two PCETs discussed above from the calculations: from $^{1}\mathbf{3}^{+0}$ to $^{2}\mathbf{7}^{+0}$, and from $^{2}\mathbf{7}^{+0}$ to $^{3}\mathbf{11}^{+0}$. Finally, the oxidation of $^{3}\mathbf{11}^{+0}$ to $^{2}\mathbf{12}^{+1}$ with a potential of -0.59 V enables the same $^{2}\mathbf{12}^{+1}$+$^{2}\mathbf{12}^{+1}$ path as found at pH = 1. We have also studied the possible formation of the compound $^{1}\mathbf{A}^{+1}$ as proposed in the work by Concepcion and coworkers [28], as well as a possible species $^{2}\mathbf{A'}^{+0}$. Gibbs energy barriers for the formation of compound $^{1}\mathbf{A}^{+1}$ of 32.7 kcal/mol ($^{2}\mathbf{7}^{+0}$+$^{2}\mathbf{12}^{+1}$) and of 41.5 kcal/mol ($^{1}\mathbf{8}^{+1}$+$^{3}\mathbf{11}^{+0}$) were found, whereas generation of $^{2}\mathbf{A'}^{+0}$ from $^{2}\mathbf{7}^{+0}$+$^{3}\mathbf{11}^{+0}$ has to overcome a Gibbs energy barrier of 26.7 kcal/mol, all these barriers to be compared with the barrier of 11.4 kcal/mol found for the $^{2}\mathbf{12}^{+1}$+$^{2}\mathbf{12}^{+1}$ coupling. All these alternative reaction paths have barriers higher in energy than the $^{2}\mathbf{12}^{+1}$+$^{2}\mathbf{12}^{+1}$ path, the rds at pH = 1. Moreover, the $^{2}\mathbf{12}^{+1}$+$^{2}\mathbf{12}^{+1}$ path is also the one showing a more favorable thermodynamics among the different I2M processes studied. Therefore, we conclude that these new proposals are less likely to be operative than the common I2M path. Therefore, our results indicate that the $^{2}\mathbf{12}^{+1}$+$^{2}\mathbf{12}^{+1}$ bimolecular step is the rds at both pHs. Furthermore, we also tried to locate the rhomboid bis(μ-oxo)-Ru$^{V}_2$ species (Scheme 1) but all our attempts lead to compound $^{1}\mathbf{13}^{+2}$. We concluded that the bis(μ-oxo)-Ru$^{V}_2$ species does not exist in the potential energy surface, probably because the sterically hindered metal center prefers an μ-η^{1}:η^{1}-peroxo-Ru$^{IV}_2$ structure rather than a bis(μ-oxo)-Ru$^{V}_2$ arrangement. Finally, the proposed reaction mechanism at pH = 8 is base-assisted in the sense that formation of $^{3}\mathbf{11}^{+0}$ is favored at this pH.

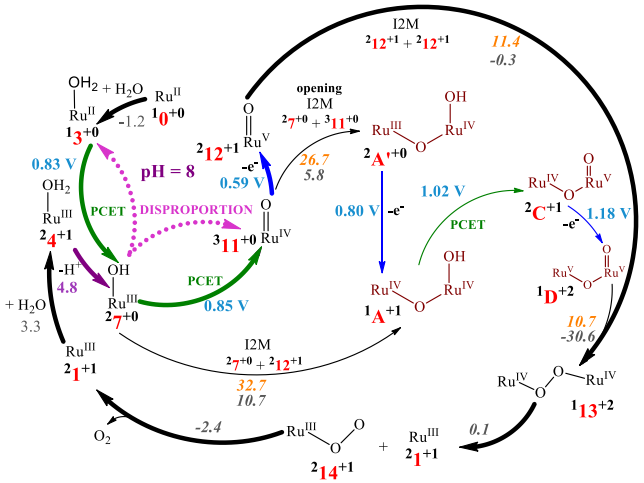

Scheme 4. Mechanism for the carboxylate catalyst at pH = 8; PCETs potentials in green; Gibbs energy barriers in orange; reduction potentials in light blue; pK_as in purple; Gibbs reaction energies in grey. Energies are given in kcal/mol and reduction potentials in V. Main path represented with bold arrows. Arrows in blue denote oxidation processes, in purple proton transfers, in green proton-coupled electron transfers and in pink and dashed disproportion processes.

CONCLUSIONS

We have explored the full mechanism for the 2,2'-bipyridine-6,6'-dicarboxylate Ru WOC catalyst at pH = 1 and 8. The most important difference in the reaction mechanisms at these two pH is the appearance of compounds $^2\mathbf{7}^{+0}$ and $^3\mathbf{11}^{+0}$ at pH = 8. This occurs because the basic pH enables the deprotonation of species $^2\mathbf{4}^{+1}$. Furthermore, experiments show that at basic pHs there is only one $2e^-/2H^+$ step. We propose that this $2e^-/2H^+$ step is the sum of the two PCETs from $^1\mathbf{3}^{+0}$ to $^2\mathbf{7}^{+0}$ and $^2\mathbf{7}^{+0}$ to $^3\mathbf{11}^{+0}$. The compounds $^2\mathbf{7}^{+0}$ and $^3\mathbf{11}^{+0}$ open new paths that may lead to the Concepcion *et al.* proposed compound $^1\mathbf{A}^{+1}$. We studied all possible dimerization processes between species involved in the mechanism and we found that the I2M $^2\mathbf{7}^{+0}$+$^3\mathbf{11}^{+0}$ to obtain $^2\mathbf{A'}^{+0}$ is lower in energy than $^2\mathbf{7}^{+0}$+$^2\mathbf{12}^{+1}$ I2M, yet both involve energy barriers higher than the $^2\mathbf{12}^{+1}$+$^2\mathbf{12}^{+1}$ I2M. Overall, we believe that at room temperature the Concepcion *et al.* proposal at pH = 8 that requires formation of $^2\mathbf{A'}^{+0}$ or $^1\mathbf{A}^{+1}$, is not possible or, at least, the reaction will be much slower than the already known path corresponding to the coupling between two Ru^V=O moieties.

AUTHOR INFORMATION

Corresponding Authors

*E-mail: miquel.sola@udg.edu, albert.poater@udg.edu

Notes

The authors declare no competing financial interest.

ACKNOWLEDGMENT

J.A.L.U. thanks Universitat de Girona for a IFUdG2017 PhD fellowship. A.P. is a Serra Húnter Fellow. A.P. and M.S. thank the Spanish MINECO for projects CTQ2014-59832-JIN and CTQ2017-85341, respectively. M.S. thanks the Generalitat de Catalunya for project 2017SGR39, the Xarxa de Referència en Química Teòrica i Computacional, and ICREA Academia 2014 prize. We thank Dr. Verònica Postils, Martí Gimferrer, Prof. Dr. Antoni Llobet, and Prof. Dr. Etsuko Fujita for helpful comments.

ABBREVIATIONS

CAN = cerium ammonium nitrate
I2M = interaction between 2 M-O sites
PCET = proton coupled electron transfer
rds = rate determining step
WNA = water nucleophilic attack
WOC = water oxidation catalysis

ASSOCIATED CONTENT

Computational details, Cartesian coordinates and energies of all species studied. This material is available free of charge via the Internet.

REFERENCES

[1] Wang, C.; Cao, S.; Fu, W. A Stable Dual-Functional System of Visible-Light-Driven Ni(II) Reduction to a Nickel Nanoparticle Catalyst and Robust in situ Hydrogen Production. *Chem. Commun.* **2013**, *49*, 11251–11253.

[2] Morris, J.; Radu, M. In situ Produced Hydrogen (Hydrogen on Demand). *Int. J. Hydrogen Energy* **2010**, *35*, 7021–7023.

[3] Silva, J. M.; Soria, M. A.; Madeira, L. M. Thermodynamic Analysis of Glycerol Steam Reforming for Hydrogen Production with in situ Hydrogen and Carbon Dioxide Separation. *J. Power Sources* **2015**, *273*, 423–430.

[4] Liu, T.; Zhang, B.; Sun, L. Iron-Based Molecular Water Oxidation Catalysts: Abundant, Cheap, and Promising. *Chem. Asian J.* **2019**, *14*, 31–43.

[5] Duan, L.; Bozoglian, F.; Mandal, S.; Stewart, B.; Privalov, T.; Llobet, A.; Sun, L. A Molecular Ruthenium Catalyst with Water-Oxidation Activity Comparable to that of Photosystem II. *Nat. Chem.* **2012**, *4*, 418–423.

[6] Schulze, M.; Kunz, V.; Frischmann, P. D.; Würthner, F. A Supramolecular Ruthenium Macrocycle with High Catalytic Activity for Water Oxidation that Mechanistically Mimics Photosystem II. *Nat. Chem.* **2016**, *8*, 576–583.

[7] Matheu, R.; Ertem, M. Z.; Gimbert-Suriñach, C.; Sala, X.; Llobet, A. Seven Coordinated Molecular Ruthenium–Water Oxidation Catalysts: A Coordination Chemistry Journey. *Chem. Rev.* **2019**, *119*, 3453–3471.

[8] Sun, L.; Hammarström, L.; Åkermark, B.; Styring, S. Towards Artificial Photosynthesis: Ruthenium-Manganese Chemistry for Energy Production. *Chem. Soc. Rev.* **2001**, *30*, 36–49.

[9] Manbeck, G. F.; Fujita, E.; Concepcion, J. J. Proton-Coupled Electron Transfer in a Strongly Coupled Photosystem II-Inspired Chromophore-Imidazole-Phenol Complex: Stepwise Oxidation and Concerted Reduction. *J. Am. Chem. Soc.* **2016**, *138*, 11536–11549.

[10] (a) Sheridan, M. V.; Sherman, B. D.; Fang, Z.; Wee, K.-R.; Coggins, M. K.; Meyer, T. J. Electron Transfer Mediator Effects in the Oxidative Activation of a Ruthenium Dicarboxylate Water Oxidation Catalyst. *ACS Catal.* **2015**, *5*, 4404–4409. (b) Tsubonouchi, Y.; Lin, S.; Parent, A. R.; Brudvig, G. W.; Sakai, K. Light-Induced Water Oxidation Catalyzed by an Oxido-Bridged Triruthenium Complex with a Ru-O-Ru-O-Ru Motif. *Chem. Commun.* **2016**, *52*, 8018–8021.

[11] Daniel, Q.; Huang, P.; Fan, T.; Wang, Y.; Duan, L.; Wanga, L.; Li, F.; Rinkevicius, Z.; Mamedov, F.; Ahlquist, M. S. G.; Styring,

S.; Sun, L. Rearranging from 6- to 7-Coordination Initiates the Catalytic Activity: An EPR Study on a Ru-bda Water Oxidation Catalyst. *Coord. Chem. Rev.* **2017**, *346*, 206–215.
[12] Concepcion, J. J.; Tsai, M.-K.; Muckerman, J. T.; Meyer, T. J. Mechanism of Water Oxidation by Single-Site Ruthenium Complex Catalysts. *J. Am. Chem. Soc.* **2010**, *132*, 1545–1557.
[13] López, I.; Ertem, M. Z.; Maji, S.; Benet-Buch, J.; Keidel, A.; Kuhlmann, U.; Hildebrandt, P.; Cramer, C. J.; Batista, V. S.; Llobet, A. A Self-Improved Water-Oxidation Catalyst: Is One Site Really Enough? *Angew. Chem. Int. Ed.* **2014**, *53*, 205–209.
[14] Vigara, L.; Ertem, M. A.; Planas, N.; Bozoglian, F.; Leidel, N.; Dau, H.; Haumann, M.; Gagliardi, L.; Cramer, C. J.; Llobet, A. Experimental and Quantum Chemical Characterization of the Water Oxidation Cycle Catalysed by $[Ru^{II}(damp)(bpy)(H_2O)]^{2+}$. *Chem. Sci.* **2012**, *3*, 2576–2586.
[15] Gersten, S. W.; Samuels, G. J.; Meyer, T. J. Catalytic Oxidation of Water by an Oxo-Bridged Ruthenium Dimer. *J. Am. Chem. Soc.* **1982**, *104*, 4029–4030.
[16] Kang, R.; Chen, K.; Yao, J.; Shaik, S.; Chen, H. Probing Ligand Effects on O-O Bond Formation of Ru-Catalyzed Water Oxidation: A Computational Survey. *Inorg. Chem.* **2014**, *53*, 7130–7136.
[17] Neudeck, S.; Maji, S.; López, I.; Meyer, S.; Meyer, F.; Llobet, A. New Powerful and Oxidatively Rugged Dinuclear Ru Water Oxidation Catalyst: Control of Mechanistic Pathways by Tailored Ligand Design. *J. Am. Chem. Soc.* **2014**, *136*, 24–27.
[18] Liao, R.-Z.; Kärkäs, M. D.; Laine, T. M.; Åkermark, B.; Siegbahn, P. E. M. On the Mechanism of Water Oxidation Catalyzed by a Dinuclear Ruthenium Complex: a Quantum Chemical Study. *Catal. Sci. Technol.* **2016**, *6*, 5031–5041.
[19] Pasha, F. A.; Poater, A.; Vummaleti, S. V. C.; de Bruin, T.; Basset, J.-M.; Cavallo, L. Revisiting O–O Bond Formation through Outer-Sphere Water Molecules versus Bimolecular Mechanisms in Water-Oxidation Catalysis (WOC) by Cp*Ir Based Complexes. *Eur. J. Inorg. Chem.* **2019**, 2093–2100.
[20] Staehle, R.; Tong, L.; Wang, L.; Duan, L.; Fischer, A.; Ahlquist, M. S. G.; Sun, L.; Rau, S. Water Oxidation Catalyzed by Mononuclear Ruthenium Complexes with a 2,2'-Bipyridine-6,6'-dicarboxylate (bda) Ligand: How Ligand Environment Influences the Catalytic Behavior. *Inorg. Chem.* **2014**, *53*, 1307–1319.
[21] (a) Xie, Y.; Shaffer, D. W.; Concepcion, J. J. O−O Radical Coupling: From Detailed Mechanistic Understanding to Enhanced Water Oxidation Catalysis. *Inorg. Chem.* **2018**, *57*, 10533–10542. (b) Zhan, S.; Ahlquist, M. S. G. Dynamics and Reactions of Molecular Ru Catalysts at Carbon Nanotube–Water Interfaces. *ACS Catal.* **2018**, *8*, 8642–8648. (c) Zhan, S., Ahlquist, M.S.G. Dynamics and Reactions of Molecular Ru Catalysts at Carbon Nanotube-Water Interfaces. *J. Am. Chem. Soc.* **2018**, *140*, 7498–7503.
[22] Scherrer, D.; Schilling, M.; Luber, S.; Fox, T.; Spingler, B.; Alberto, R.; Richmond, C. J. Ruthenium Water Oxidation Catalysts Containing the Non-Planar Tetradentate Ligand, Biisoquinoline Dicarboxylic Acid ($biqaH_2$). *Dalton Trans.* **2016**, *45*, 19361–19367.
[23] Tong, L.; Duan, L. Xu, Y.; Privalov, T.; Sun, L. Structural Modifications of Mononuclear Ruthenium Complexes: A Combined Experimental and Theoretical Study on the Kinetics of Ruthenium Catalyzed Water Oxidation. *Angew. Chem. Int. Ed.* **2011**, *50*, 445–449.
[24] Matheu, R.; Ertem, M. Z.; Pipelier, M.; Lebreton, J.; Dubreuil, D.; Benet-Buchholz, J.; Sala, X.; Tessier, A.; Llobet, A. The Role of Seven-Coordination in Ru-Catalyzed Water Oxidation. *ACS Catal.* **2018**, *8*, 2039–2048.
[25] Zhang, B.; Sun, L. Ru-bda: Unique Molecular Water-Oxidation Catalysts with Distortion Induced Open Site and Negatively Charged Ligands. *J. Am. Chem. Soc.* **2019**, *141*, 5565–5580.
[26] Sala, X.; Romero, I.; Rodríguez, M.; Escriche, L.; Llobet, A. Molecular Catalysts that Oxidize Water to Dioxygen. *Angew. Chem. Int. Ed.* **2009**, *48*, 2842–2852.
[27] Govindarajan, N.; Tiwari, A.; Ensing, B.; Meijer, E. J. Impact of the Ligand Flexibility and Solvent on the O–O Bond Formation

Step in a Highly Active Ruthenium Water Oxidation Catalyst. *Inorg. Chem.* **2018**, *57*, 13063–13066.
[28] Concepcion, J. J.; Zhong, D. K.; Szalda, D. J.; Muckerman, J. T.; Fujita, E. Mechanism of Water Oxidation by [Ru(bda)(L)$_2$]: the Return of the Blue Dimer. *Chem. Commun.* **2015**, *51*, 4105–4108.
[29] Muckerman, J. T.; Kowalczyk, M.; Badiei, Y. M.; Polyansky, D. E.; Concepcion, J. J.; Zong, R.; Thummel, R. P.; Fujita, E. New Water Oxidation Chemistry of a Seven-Coordinate Ruthenium Complex with a Tetradentate Polypyridyl Ligand. *Inorg. Chem.* **2014**, *53*, 6904–6913.
[30] Zhan, S.; Martensson, D.; Purg, M.; Kamerlin, S. C. L.; Ahlquist, M. S. G. Capturing the Role of Explicit Solvent in the Dimerization of Ru^{V}(bda) Water Oxidation Catalysts. *Angew. Chem. Int. Ed.* **2017**, *56*, 6962–6965.
[31] Shaffer, D. W.; Xie, Y.; Concepcion, J. J. O–O Bond Formation in Ruthenium-Catalyzed Water Oxidation: Single-Site Nucleophilic Attack vs. O–O Radical Coupling. *Chem. Soc. Rev.* **2017**, *46*, 6170–6193.
[32] Gaussian 09, Revision E.01, Frisch, M. J.; Trucks, G. W.; Schlegel, H. B.; Scuseria, G. E.; Robb, M. A.; Cheeseman, J. R.; Scalmani, G.; Barone, V.; Mennucci, B.; Petersson, G. A.; Nakatsuji, H.; Caricato, M.; Li, X.; Hratchian, H. P.; Izmaylov, A. F.; Bloino, J.; Zheng, G.; Sonnenberg, J. L.; Hada, M.; Ehara, M.; Toyota, K.; Fukuda, R.; Hasegawa, J.; Ishida, M.; Nakajima, T.; Honda, Y.; Kitao, O.; Nakai, H.; Vreven, T.; Montgomery, J. A., Jr.; Peralta, J. E.; Ogliaro, F.; Bearpark, M.; Heyd, J. J.; Brothers, E.; Kudin, K. N.; Staroverov, V. N.; Kobayashi, R.; Normand, J.; Raghavachari, K.; Rendell, A.; Burant, J. C.; Iyengar, S. S.; Tomasi, J.; Cossi, M.; Rega, N.; Millam, N. J.; Klene, M.; Knox, J. E.; Cross, J. B.; Bakken, V.; Adamo, C.; Jaramillo, J.; Gomperts, R.; Stratmann, R. E.; Yazyev, O.; Austin, A. J.; Cammi, R.; Pomelli, C.; Ochterski, J. W.; Martin, R. L.; Morokuma, K.; Zakrzewski, V. G.; Voth, G. A.; Salvador, P.; Dannenberg, J. J.; Dapprich, S.; Daniels, A. D.; Farkas, Ö.; Foresman, J. B.; Ortiz, J. V.; Cioslowski, J.; Fox, D. J. Gaussian, Inc., Wallingford CT, **2009**.
[33] Zhao, Y.; Truhlar D. G. The M06 Suite of Density Functionals for Main Group Thermochemistry, Thermochemical Kinetics, Noncovalent Interactions, Excited States, and Transition Elements: Two New Functionals and Systematic Testing of Four M06-Class Functionals and 12 Other Functionals. *Theor. Chem. Acc.* **2008**, *120*, 215–241.
[34] Zhao, Y.; Truhlar, D. G. A New Local Density Functional for Main-Group Thermochemistry, Transition Metal Bonding, Thermochemical Kinetics, and Noncovalent Interactions. *J. Chem. Phys.* **2006**, *125*, 194101:1–18.
[35] Schäfer, A.; Horn, H.; Ahlrichs, R. Fully Optimized Contracted Gaussian Basis Sets for Atoms Li to Kr. *J. Chem. Phys.* **1992**, *97*, 2571–2577.
[36] Haeusermann, U.; Dolg, M.; Stoll, H.; Preuss, H. Accuracy of Energy-Adjusted Quasirelativistic Ab Initio Pseudopotentials. *Mol. Phys.* **1993**, *78*, 1211–1224.
[37] Martin, R. L.; Hay, P. J.; Pratt, L. R. Hydrolysis of Ferric Ion in Water and Conformational Equilibrium. *J. Phys. Chem. A* **1998**, *102*, 3565–3573.
[38] (a) García-Melchor, M.; Pacheco, M. C.; Nájera, C.; Lledós, A.; Ujaque, G. Mechanistic Exploration of the Pd-Catalyzed Copper-Free Sonogashira Reaction. *ACS Catal.* **2012**, *2*, 135–144. (b) Poater, A.; Pump, E.; Vummaleti, S. V. C.; Cavallo, L. The Right Computational Recipe for Olefin Metathesis with Ru-Based Catalysts: the Whole Mechanism of Ring-Closing Olefin Metathesis. *J. Chem. Theory Comput.* **2014**, *10*, 4442–4448. (c) Falivene, L.; Barone, V.; Talarico, G. Unraveling the Role of Entropy in Tuning Unimolecular vs. Bimolecular Reaction Rates: The Case of Olefin Polymerization Catalyzed by Transition Metals. *Mol. Catal.* **2018**, *452*, 138–144.
[39] Weigend, F.; Ahlrichs, R. Balanced Basis Set of Split Valence, Triple Zeta Valence and Quadruple Zeta Valence Quality for H to Rn: Design and Assessment of Accuracy. *Phys. Chem. Chem. Phys.* **2005**, *7*, 3297–3305.
[40] Barone, V.; Cossi, M. Quantum Calculation of Molecular Energies and Energy Gradients in Solution by a Conductor Solvent Model. *J. Phys. Chem. A* **1998**, *102*, 1995–2001.
[41] Tomasi, J.; Persico, M. Molecular Interactions in Solution: An Overview of Methods Based on Continuous Distributions of the Solvent. *Chem. Rev.* **1994**, *94*, 2027–2094.
[42] Durrant, M. C.; Gilson, R. Estimation of the pK_a Values of Water Ligands in Transition Metal Complexes Using Density Functional Theory with Polarized Continuum Model Solvent Corrections. *Dalton Trans.* **2009**, 10223–10230.
[43] Kamdar, J. M.; Marelius, D. C.; Moore, C. E.; Rheingold, A. L.; Smith, D. K.; Grotjahn, D. B. Ruthenium complexes of 2,2'-bipyridine-6,6'-diphosphonate ligands for water oxidation. *ChemCatChem* **2016**, *8*, 3045–3049.
[44] Acuña-Parés, F.; Codolà, Z.; Costas, M.; Luis, J. M.; Lloret-Fillol, J. Unraveling the Mechanism of Water Oxidation Catalyzed by Nonheme Iron Complexes. *Chem. Eur. J.* **2014**, *20*, 5696–5707.
[45] Kelly, C. P.; Cramer, C. J.; Truhlar, D. G. Single-Ion Solvation Free Energies and the Normal Hydrogen Electrode Potential in Methanol, Acetonitrile, and Dimethyl Sulfoxide. *J. Phys. Chem. B* **2007**, *111*, 408–422.
[46] (a) Nernst, W. The New Heat Theorem; Dover: New York, 1969. (b) Feiner, A.-S.; McEvoy, A. J. The Nernst Equation. *J. Chem. Educ.* **1994**, *71*, 493–494.
[47] (a) Ramos-Cordoba, E.; Postils, V.; Salvador, P. Oxidation States from Wave Function Analysis. *J. Chem. Theory Comput.* **2015**, *11*, 1501–1508. (b) Skara, G.; Gimferrer, M.; De Proft, F.; Salvador, P.; Pinter, B. Scrutinizing the Noninnocence of Quinone Ligands in Ruthenium Complexes: Insights from Structural, Electronic, Energy, and Effective Oxidation State Analyses. *Inorg. Chem.* **2016**, *55*, 2185–2199. (c) Poater, J.; Gimferrer, M.; Poater, A. Covalent and Ionic Capacity of MOFs To Sorb Small Gas Molecules. *Inorg. Chem.* **2018**, *57*, 6981–6990.
[48] (a) Ertem, M. Z.; Gagliardi, L.; Cramer, C. J. Quantum Chemical Characterization of the Mechanism of an Iron-Based Water Oxidation Catalyst. *Chem. Sci.* **2012**, *3*, 1293–1299. (b) Bucci, A.; Menendez Rodriguez, G.; Bellachioma, G.; Zuccaccia, C.; A. Poater, A.; Cavallo, L.; Macchioni, A. An Alternative Reaction Pathway for Iridium-Catalyzed Water Oxidation Driven by Cerium Ammonium Nitrate (CAN). *ACS Catal.* **2016**, *6*, 4559–4563.
[49] Wadsworth, E.; Duke, F. R.; Goetz, C. A. Present Status of Cerium(IV)-Cerium(III) Potentials. *Anal. Chem.* **1957**, *29*, 1824–1825.
[50] Shaffer, D. W.; Xie, Y.; Szalda, D. J.; Concepcion, J. J. Manipulating the Rate-Limiting Step in Water Oxidation Catalysis by Ruthenium Bipyridine−Dicarboxylate Complexes. *Inorg. Chem.* **2016**, *55*, 12024−12035.
[51] Lebedev, D.; Pineda-Galvan, Y.; Tokimaru, Y.; Fedorov, A.; Kaeffer, N.; Copéret, C.; Pushkar, Y. The Key Ru^{V}=O Intermediate of Site-Isolated Mononuclear Water Oxidation Catalyst Detected by in Situ X-ray Absorption Spectroscopy. *J. Am. Chem. Soc.* **2018**, *140*, 451−458.
[52] Richmond, C. J.; Escayola, S.; Poater, A. Axial Ligand Effects of Ru-BDA Complexes in the O–O Bond Formation via the I2M Bimolecular Mechanism in Water Oxidation Catalysis. *Eur. J. Inorg. Chem.* **2019**, 2093–2100.
[53] (a) Richmond, C. J.; Matheu, R.; Poater, A.; Falivene, L.; Benet-Buchholz, J.; Sala, X.; Cavallo, L.; Llobet, A. Supramolecular Water Oxidation with Ru-bda-Based Catalysts. *Chem. Eur. J.* **2014**, *20*, 17282–17286. (b) Matheu, R.; Ghaderian, A.; Francàs, L; Chernev, P.; Ertem, M. Z.; Benet-Buchholz, J.; Batista, V. S.; Haumann, M.; Gimbert-Suriñach, C.; Sala, X.; Llobet, A. Behavior of Ru–bda Water-Oxidation Catalysts in Low Oxidation States. *Chem. Eur. J.* **2018**, *24*, 12838–12847.
[54] Shaffer, D. W.; Xie, Y.; Szalda, D. J.; Concepción, J. J. Manipulating the Rate-Limiting Step in Water Oxidation Catalysis by Ruthenium Bipyridine−Dicarboxylate Complexes. *Inorg. Chem.* **2016**, *55*, 12024–12035.

[55] Zhang, B.; Li, F.; Zhang, R.; Ma, C.; Chen, L.; Sun, L. Characterization of a Trinuclear Ruthenium Species in Catalytic Water Oxidation by Ru(bda)$(pic)_2$ in Neutral Media. *Chem. Commun.* **2016**. *52*, 8619–8622.